Test for descriptions of relativistic spin dynamics by using ultraintense lasers

J. Wang,[1] X. B. Li,[1] L. F. Gan,[1,*] C. T. Zhou,[2] S. P. Zhu,[3] X. T. He,[1,2,3] and B. Qiao[1,†]

[1]*Center for Applied Physics and Technology, HEDPS, and SKLNPT, School of Physics, Peking University, Beijing 100871, China*

[2]*Shenzhen Key Laboratory of Ultraintense Laser and Advanced Material Technology, Center for Advanced Material Diagnostic Technology, and College of Engineering Physics, Shenzhen Technology University, Shenzhen 518118, China*

[3]*Institute of Applied Physics and Computational Mathematics, Beijing 100094, China*

(Received 27 April 2021; revised 19 July 2021; accepted 4 August 2021; published 17 August 2021)

The relativistic spin operator cannot be uniquely defined within relativistic quantum mechanics. Searching for relativistic equations that describe both the evolution of the spin and its influence on the motion of particles with spin represents a problem with almost centenary history. We develop a self-consistent module for modeling relativistic particles with spin motion into three-dimensional particle-in-cell simulations, where the expression of the spin-induced force can be chosen by various semiclassical models, such as the Frenkel and noncovariant Derbenev-Kondratenko models. Through simulations, we propose a potential experimental scheme for observing and testing theoretical descriptions on relativistic spin dynamics, where ultraintense lasers are used to collide with relativistic electron beams. The basis for the scheme is that different models predict different transverse polarization distributions of the scattered electrons after interactions, which can be measured in experiments.

DOI: 10.1103/PhysRevA.104.023104

I. INTRODUCTION

The Nobel Prize in Physics 2018 was half awarded to Gérard Mourou and Donna Strickland for their chirped pulse amplification (CPA) technique [1] of generating short-pulse ultraintense lasers. One groundbreaking application of the CPA invention is offering the possibility of a new experimental window into the largely unexplored world of strong field quantum electrodynamics (QED) by using lasers with unprecedented intensities. In view of this, many ultrahigh-power laser facilities are under construction such as Extreme Light Infrastructure (ELI) [2], Vulcan [3], Exawatt Center for Extreme Light Studies (XCELS) [4], and Shanghai Superintense Ultrafast Laser Facility (SULF) [5]. One of the most important motivations of QED experiments using ultraintense lasers is to achieve sufficiently clear observation of various QED effects, allowing for detailed tests and comparison with QED theoretical predictions that generally provide only unobservable probabilities.

Spin, as an intrinsic property of elementary particles, occupies a crucial position in QED [6–9]. In the nonrelativistic regime, the spin dynamics can be simply described by the nonrelativistic quantum mechanics (QM) [10], where the spin is defined by the 2×2 Pauli matrices σ_i $(i = 1, 2, 3)$, corresponding to the classical spin vector $\mathbf{s}$, whose components represent the expectation values of the spin along each of the axes. Basic notions of special and general relativity have been formulated before the discovery of spin, so they describe the properties of space and time as they are seen by spinless particles. It is natural to ask whether these notions remain the same if the spinless particle is replaced by a more realistic particle with spin. Searching for the relativistic equations that describe both the evolution of the particle spin and its influence on the motion of a particle with spin represents a critical issue with almost centenary history [11–22].

In principle, spin is naturally introduced into dynamics of relativistic electrons through the Dirac equation [9]. However, the key issue is that there is no universally accepted spin operator in the relativistic regime [23–28], resulting in obscureness of spin-related theories sourced from relativistic quantum mechanics [29–32]. Thus more intuitive semiclassical models based on relativistic generalization of the nonrelativistic semiclassical spin model have attracted more attention because the problem of the nonunique relativistic spin operator is circumvented. For the evolution of relativistic spin, the precession of spin of relativistic electrons in uniform fields is described as the Thomas-Bargmann-Michel-Telegdi (T-BMT) equation [8], which is commonly used in recent studies on generation of polarized relativistic particle beams by ultraintense lasers [33–41]. However, more essentially, the reverse effect of the spin on trajectories of relativistic particles in such laser fields is often ignored and still not understood. In fact, based on different considerations, the spin-induced force, namely, the Stern-Gerlach (SG) force [42], can be derived as different forms in various models, such as the Frenkel model [16,22], the noncovariant Derbenev-Kondratenko (DK) model [7,15,17,43], and so on [18,44,45]. Thus it is necessary to test whether various spin models are still valid in the presence of ultraintense laser fields. Recently, the Frenkel model and Foldy-Wouthuysen model have been numerically benchmarked against each other and the Dirac equation for single-particle motion in a strong laser pulse [46]; however, more work needs to be done to investigate the validity of

*Corresponding author: lfgan@pku.edu.cn
†Corresponding author: bqiao@pku.edu.cn

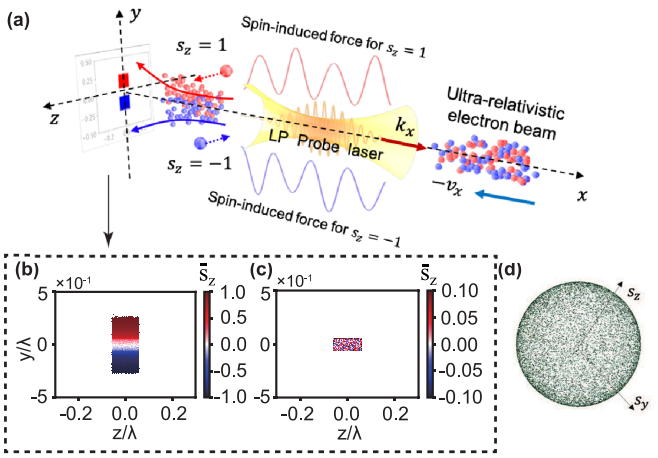

FIG. 1. (a) Schematic of the proposed scheme for testing theoretical predictions of different semiclassical models. Red and blue spheres represent electrons polarized parallel and antiparallel to the z direction, respectively. (b) and (c) Transverse spatial distributions of the polarizations of scattered electrons in simulations with the Frenkel and noncovariant DK models, respectively. (d) Initial polarization distribution of the electron beam.

the models, especially concerning collective effects, radiation reaction (RR), etc.

In this paper, in view of the above concerns, we develop a self-consistent module for describing the motion of a particle with spin in three-dimensional (3D) particle-in-cell (PIC) simulations [47], where the SG force can be chosen based on various semiclassical models, such as the above Frenkel model and noncovariant DK model and others given in Appendix A. Based on simulations with this capability, we propose a potential experimental scheme for testing theoretical predictions of different models, where a linearly polarized (LP) ultraintense laser is used to interact with a relativistic electron beam, as shown in the schematic in Fig. 1(a). It is found that different models predict different transverse polarization distributions of the scattered electrons after interactions in the scheme, which can be measured in experiments. If the Frenkel model is used, the electron beam can be separated spatially into two parts with opposite transverse polarizations, shown in Fig. 1(b), which, however, does not appear once the noncovariant DK model is applied, shown in Fig. 1(c). As mentioned above, the reason for this distinction comes from different considerations in the establishment of these models. On the one hand, the noncovariant DK model stems from the Lagrangian with approximation of uniform fields, whereas the Frenkel model does not. On the other hand, equations in the Frenkel model are covariant and can be reduced to those in the rest system, which is not guaranteed in the noncovariant DK model (see Secs. II B and II C for the establishment of the models in detail).

II. THEORETICAL ANALYSIS

A. Relativistic generalizations of classical spin vector s

As we know, the spin of a particle can be described as a vector $\mathbf{s}$ with a length of $|\mathbf{s}| = \hbar/2$ in the rest frame, whose components represent the probability that the electron is in the corresponding spin state. Analogous to some dynamic quantities, there are several generalizations of this spin vector in the relativistic regime.

One of alternatives is to use a four-vector $S^\mu(S_0, \mathbf{S})$ as a covariant description of spin in the laboratory frame, whose independent components $\mathbf{S}$ will reduce to the spin vector $\mathbf{s}$ in the particle's rest frame. According to the Lorentz transformation, covariant constraint $U_\mu S^\mu = 0$ can be obtained, where $U_\mu = \gamma(c, -\boldsymbol{v})$ is the particle's four-velocity; $\gamma = (1 - v^2/c^2)^{-1/2}$ is the Lorentz factor of the particle. Connections between components of S^μ and $\mathbf{s}$ are displayed as

$$\begin{aligned} \mathbf{S} &= \mathbf{s} + \frac{\gamma^2}{\gamma + 1}(\boldsymbol{\beta} \cdot \mathbf{s})\boldsymbol{\beta}, \\ S_0 &= \boldsymbol{\beta} \cdot \mathbf{S} = \gamma \boldsymbol{\beta} \cdot \mathbf{s}, \end{aligned} \tag{1}$$

where $\beta = \boldsymbol{v}/c$ is the normalized velocity of the particle.

In addition, an antisymmetric tensor $S^{\alpha\beta} = (\mathbf{m}, \mathbf{d})$, first proposed by Frenkel in 1926 [16], can also be considered as a relativistic generalization of the spin vector:

$$\mathrm{S}^{\alpha\beta} = \begin{pmatrix} 0 & -d_x & -d_y & -d_z \\ d_x & 0 & m_z & -m_y \\ d_y & -m_z & 0 & m_x \\ d_z & m_y & -m_x & 0 \end{pmatrix}, \tag{2}$$

where $\mathbf{m}$ is equal to spin vector $\mathbf{s}$ in the particle's rest frame and $\chi\mathbf{m}$ and $\chi\mathbf{d}$ correspond to the magnetic moment and electric dipole moment, respectively. Here, $\chi = qg_s/2m_0$; q and m_0 are the charge and the mass of the particle, and g_s is called the spin g factor. Based on the requirements $S^{\alpha\beta}U_\beta = 0$ and $\frac{1}{2}S^{\alpha\beta}S_{\alpha\beta} = \mathbf{s}^2$, the relationship between the components of the Frenkel tensor and spin vector can be obtained as

$$\begin{aligned} \mathbf{m} &= \gamma \mathbf{s} - \frac{\gamma^2}{\gamma + 1}(\boldsymbol{\beta} \cdot \mathbf{s})\boldsymbol{\beta}, \\ \mathbf{d} &= \boldsymbol{\beta} \times \mathbf{m} = \gamma \boldsymbol{\beta} \times \mathbf{s}. \end{aligned} \tag{3}$$

B. Equation of motion of the Frenkel model

The proposal of the Frenkel model is based on regarding $S^{\alpha\beta} = (\mathbf{m}, \mathbf{d})$ as the relativistic generalization of the spin vector in the rest frame. Considering the interaction between spin and the electromagnetic (EM) field, the Lagrangian of a particle with mass m_0 and charge q can be expressed as [16]

$$\mathcal{L} = MU_\alpha U^\alpha + qA_\alpha U^\alpha + T^* + \frac{\chi}{2}S^{\alpha\beta}F_{\alpha\beta} + \chi a_\alpha S^{\alpha\beta}U_\beta, \tag{4}$$

where $A_\alpha = (\phi/c, -\mathbf{A})$ and $F_{\alpha\beta} = \partial_\alpha A_\beta - \partial_\beta A_\alpha$ are the four-potential and tensor of the EM field, respectively. T^* represents the "rotational energy" of the particle's spin, and the fourth term is the "spin-field interaction energy." Here, $M = m_0 + m'$ and a_α are introduced as Lagrangian multipliers to ensure satisfaction of the on-shell condition $U^\alpha U_\alpha = c^2$ and $S^{\alpha\beta}U_\beta = 0$, which can be determined below. According to the least action principle $\int \delta\mathcal{L}d\tau = 0$, the orbital motion equation

and spin precession equation can be derived consistently as [16,22]

$$M\dot{U}_\alpha = qF_{\alpha\beta}U^\beta + \frac{\chi}{2}S^{\gamma\beta}\left(\frac{\partial}{\partial x^\alpha} - \frac{1}{c^2}U_\alpha U^\beta\frac{\partial}{\partial x^\beta}\right)F_{\gamma\beta} + R_\alpha, \tag{5}$$

$$\dot{S}^{\alpha\beta} = \chi\left(F^\alpha_\sigma S^{\sigma\beta} - F^\beta_\sigma S^{\sigma\alpha}\right) + \chi a_\gamma(U^\alpha S^{\beta\gamma} - U^\beta S^{\alpha\gamma}), \tag{6}$$

where the dot means taking a derivative with respect to proper time τ and $a_\gamma = -(\chi F_{\gamma\alpha}U^\alpha - \dot{U}_\gamma)/\chi c^2$. The spin-induced effective mass $M = m_0 + \frac{\chi}{2c^2}S^{\beta\gamma}F_{\beta\gamma}$, which can be regarded as the dressed mass due to the interaction between spin and fields; there is a similar expression for it that follows from the Dirac-Pauli equation [22,48,49]. $R_\alpha = -\chi[U_\alpha\dot{S}^{\beta\gamma}F_{\beta\gamma}/2c^2 + \dot{a}_\beta S^\beta_\alpha + a_\beta\dot{S}^\beta_\alpha]$ can be seen as a vector that has no physical meaning when considering the requirement $m_0\dot{\boldsymbol{v}} = q\mathbf{E} + \chi\nabla(\mathbf{s}\cdot\mathbf{B})$ in the particle's rest frame [22]. Thus the Frenkel model gives a relativistic equation in covariant form that describes the influence of spin on the particle's motion:

$$M\dot{U}_\alpha = qF_{\alpha\beta}U^\beta + \frac{\chi}{2}S^{\gamma\beta}\left(\frac{\partial}{\partial x^\alpha} - \frac{1}{c^2}U_\alpha U^\beta\frac{\partial}{\partial x^\beta}\right)F_{\gamma\beta}, \tag{7}$$

where the spatial components are written as

$$\left[m_0 - \frac{\chi}{c^2}\left(\mathbf{m}\cdot\mathbf{B} + \frac{\mathbf{d}\cdot\mathbf{E}}{c}\right)\right]\frac{d(\gamma\boldsymbol{v})}{dt} = q(\mathbf{E} + \boldsymbol{v}\times\mathbf{B}) + \frac{\chi}{\gamma}\left[\nabla + \frac{\gamma^2}{c^2}\boldsymbol{v}\left(\frac{\partial}{\partial t} + \boldsymbol{v}\cdot\nabla\right)\right] \times\left(\mathbf{m}\cdot\mathbf{B} + \frac{\mathbf{d}\cdot\mathbf{E}}{c}\right), \tag{8}$$

where $\mathbf{m}\cdot\mathbf{B} + \mathbf{d}\cdot\mathbf{E}/c = \mathbf{s}\cdot[\gamma\mathbf{B} - \gamma(\boldsymbol{\beta}\times\mathbf{E})/c - \gamma^2(\boldsymbol{\beta}\cdot\mathbf{B})\boldsymbol{\beta}/(\gamma+1)]$ and the spatial gradient and temporal derivative on the right-hand side only act on EM fields ($\mathbf{E}$ and $\mathbf{B}$). It can be seen from the above equation that the influence of spin-field interaction on the electron trajectory includes spatial gradient and temporal (and spatial) variations of EM fields, in addition to the correction of the Lorentz force caused by the spin-induced effective mass.

C. Equation of motion of the noncovariant Derbenev-Kondratenko model

1. Source of the Derbenev-Kondratenko Hamiltonian

As we know, in uniform or slowly varying external fields, the relativistic covariant equation that describes the evolution of spin has been represented by the spin four-vector S^α as [50]

$$\frac{dS^\alpha}{d\tau} = \frac{q}{m_0}\left[\frac{g_s}{2}F^{\alpha\beta}S_\beta + \frac{1}{c^2}\left(\frac{g_s}{2} - 1\right)U^\alpha(S_\lambda F^{\lambda\mu}U_\mu)\right], \tag{9}$$

which is the well-known T-BMT equation [8]. Note that Eq. (6) also describes the evolution of spin in the relativistic regime. When also considering uniform or slowly varying external fields as in the T-BMT equation, i.e., substituting $\dot{U}_\gamma = qF_{\gamma\beta}U^\beta/m_0$ into a_γ of Eq. (6), Eq. (6) has been proven to be equivalent to Eq. (9) [22], by applying the dual relationship between S^μ and $S^{\alpha\beta}$, $S^\mu = \epsilon^{\mu\nu\alpha\beta}U_\nu S_{\alpha\beta}/2c$, where $\epsilon^{\mu\nu\alpha\beta}$ is the Levi-Civita symbol. According to Eqs. (9) and (1), the evolution of the spin vector $\mathbf{s}$ is given as

$$d\mathbf{s}/dt = \mathbf{s}\times\boldsymbol{\Omega}, \tag{10}$$

where $\boldsymbol{\Omega} = q\{(a+1/\gamma)\mathbf{B} - a\gamma(\boldsymbol{\beta}\cdot\mathbf{B})\boldsymbol{\beta}/(\gamma+1) - [a+1/(\gamma+1)]\boldsymbol{\beta}\times\mathbf{E}/c\}/m_0$ and $a = g_s/2 - 1$. For the nonrelativistic system, the Hamiltonian of interaction between spin and magnetic fields is $H_{\rm int} = \chi\mathbf{s}\cdot\mathbf{B}$, and the corresponding Heisenberg equation for the evolution of spin is expressed as $\frac{d\mathbf{s}}{dt} = \frac{i}{\hbar}[H_{\rm int}, \mathbf{s}] = \chi\mathbf{s}\times\mathbf{B}$. As a relativistic generalization of the above nonrelativistic equation, the T-BMT equation can also be regarded as being obtained from an effective Hamiltonian [7], as follows as in the nonrelativistic regime. Evidently, this effective Hamiltonian is

$$H^{\rm eff}_{\rm int} = q\mathbf{s}\cdot\{(a+1/\gamma)\mathbf{B} - a\gamma(\boldsymbol{\beta}\cdot\mathbf{B})\boldsymbol{\beta}/(\gamma+1) - [a+1/(\gamma+1)]\boldsymbol{\beta}\times\mathbf{E}/c\}/m_0. \tag{11}$$

It is worth mentioning that such an effective Hamiltonian can also be consistently obtained based on Foldy-Wouthuysen transformation of the Dirac Hamiltonian, where only first-order terms of spin are preserved [30].

2. Equations of motion derived by the effective Hamiltonian

According to the above effective Hamiltonian $H^{\rm eff}_{\rm int}$, another relativistic spin model can be derived by considering the Lagrangian of the interaction between the spin and EM fields as $-H^{\rm eff}_{\rm int}$. By applying the Lagrangian equation $\nabla L = \frac{d}{dt}(\frac{\partial}{\partial\mathbf{v}}L)$, the equation of motion of particles is given as follows [43]:

$$m_0\frac{d(\gamma\boldsymbol{v})}{dt} = q(\mathbf{E} + \boldsymbol{v}\times\mathbf{B}) + \mathbf{F}_{\rm SG},$$
$$\mathbf{F}_{\rm SG} = \nabla(\mathbf{s}\cdot\boldsymbol{\Omega}) - \left(\frac{d}{dt}\frac{\partial\boldsymbol{\Omega}}{\partial\boldsymbol{v}}\right)\cdot\mathbf{s} - \frac{\partial\boldsymbol{\Omega}}{\partial\boldsymbol{v}}\cdot(\mathbf{s}\times\boldsymbol{\Omega}). \tag{12}$$

Here, $\mathbf{F}_{\rm SG}$ is the so-called SG force, whose first and third terms are related to the spatial gradient of the EM fields and the change rate of the spin, respectively. The second term consists of temporal derivatives for fields ($\mathcal{T}$), energy ($\mathcal{E}$), and velocity ($\mathcal{V}$) of particles, i.e., $(\frac{d}{dt}\frac{\partial\boldsymbol{\Omega}}{\partial\boldsymbol{v}})\cdot\mathbf{s} = \mathcal{T} + \mathcal{E} + \mathcal{V}$, which can be expressed in detail as

$$\mathcal{T} = \frac{q}{m_0}\left[-\frac{\frac{d\mathbf{B}}{dt}\cdot\mathbf{s}}{\gamma^2} - \frac{a(\boldsymbol{v}\cdot\frac{d\mathbf{B}}{dt})\boldsymbol{v}\cdot\mathbf{s}}{(\gamma+1)^2c^2} + \frac{(\boldsymbol{v}\times\frac{d\mathbf{E}}{dt})\cdot\mathbf{s}}{(\gamma+1)^2c^2}\right]\frac{\gamma^3\boldsymbol{v}}{c^2} + \frac{q}{m_0}\left\{-\frac{a\gamma}{(\gamma+1)c^2}\left[\frac{d\mathbf{B}}{dt}(\boldsymbol{v}\cdot\mathbf{s}) + \left(\boldsymbol{v}\cdot\frac{d\mathbf{B}}{dt}\right)\mathbf{s}\right] + \left(a + \frac{1}{1+\gamma}\right)\frac{\mathbf{s}\times\frac{d\mathbf{E}}{dt}}{c^2}\right\}, \tag{13a}$$

$$\mathcal{E} = \frac{q}{m_0}\left[\frac{\mathbf{B}\cdot\mathbf{s}}{\gamma^3} + \frac{a(\boldsymbol{v}\cdot\mathbf{B})\boldsymbol{v}\cdot\mathbf{s}}{(\gamma+1)^3c^2} - \frac{(\boldsymbol{v}\times\mathbf{E})\cdot\mathbf{s}}{(\gamma+1)^3c^2}\right]\frac{2\gamma^3\boldsymbol{v}}{c^2}\dot{\gamma} + \frac{q}{m_0}\left[-\frac{\mathbf{B}\cdot\mathbf{s}}{\gamma^2} - \frac{a(\boldsymbol{v}\cdot\mathbf{B})\boldsymbol{v}\cdot\mathbf{s}}{(\gamma+1)^2c^2} + \frac{(\boldsymbol{v}\times\mathbf{E})\cdot\mathbf{s}}{(\gamma+1)^2c^2}\right]\frac{3\gamma^2\boldsymbol{v}}{c^2}\dot{\gamma} + \frac{q}{m_0}\left[-\frac{a(\boldsymbol{v}\cdot\mathbf{s})\mathbf{B}}{(\gamma+1)^2c^2} - \frac{a(\boldsymbol{v}\cdot\mathbf{B})\mathbf{s}}{(\gamma+1)^2c^2} - \frac{\mathbf{s}\times\mathbf{E}}{(1+\gamma)^2c^2}\right]\dot{\gamma}, \tag{13b}$$

$$\mathcal{V} = \frac{q}{m_0}\left[-\frac{a(\dot{\boldsymbol{v}}\cdot\mathbf{B})\boldsymbol{v}\cdot\mathbf{s}}{(\gamma+1)^2c^2} - \frac{a(\boldsymbol{v}\cdot\mathbf{B})\dot{\boldsymbol{v}}\cdot\mathbf{s}}{(\gamma+1)^2c^2} + \frac{(\dot{\boldsymbol{v}}\times\mathbf{E})\cdot\mathbf{s}}{(\gamma+1)^2c^2}\right]\frac{\gamma^3\boldsymbol{v}}{c^2} + \frac{q}{m_0}\left[-\frac{\mathbf{B}\cdot\mathbf{s}}{\gamma^2} - \frac{a(\boldsymbol{v}\cdot\mathbf{B})\boldsymbol{v}\cdot\mathbf{s}}{(\gamma+1)^2c^2} + \frac{(\boldsymbol{v}\times\mathbf{E})\cdot\mathbf{s}}{(\gamma+1)^2c^2}\right]\frac{\gamma^3}{c^2}\dot{\boldsymbol{v}} + \frac{q}{m_0}\left[-\frac{a\gamma(\dot{\boldsymbol{v}}\cdot\mathbf{s})\mathbf{B}}{(\gamma+1)c^2} - \frac{a\gamma(\dot{\boldsymbol{v}}\cdot\mathbf{B})\mathbf{s}}{(\gamma+1)c^2}\right], \tag{13c}$$

where the dot means taking a derivative with respect to time t and $\dot{\gamma} = q(\boldsymbol{v}\cdot\mathbf{E})/m_0c^2$ and $\dot{v} = q[\mathbf{E} + \boldsymbol{v}\times\mathbf{B} - (\boldsymbol{\beta}\cdot\mathbf{E})\boldsymbol{\beta}]/\gamma m_0$ can be substituted. It must be emphasized that the above-mentioned equation of motion including spin to first order has been proposed for a long time [17] and it is completely relativistic, but not covariant [15].

D. Comparisons of the spin-induced trajectory for ultrarelativistic electrons dominated by different models in an ultraintense laser field

Consider a LP plane-wave laser which propagates along the x axis, with $E_y = E_0\sin(k_0x - \omega_0t)$ and $B_z = B_0\sin(k_0x - \omega_0t)$, where ω_0 is the frequency and $\mathbf{k} = (k_0, 0, 0)$ is the wave vector. Thus the normalized amplitude of the laser is $a_0 = eE_0/m\omega_0c$, where e and m are the charge and mass of electrons. Then an electron with spin $\mathbf{s} = (0, 0, s_z)$ and initial velocity $\boldsymbol{v} = (-v_x, 0, 0)$ collides with the laser. It is worth mentioning that, for the circumstance we considered, different SG forces in the two semiclassical models will make the motion of the electron different in the laser polarization direction, i.e., the y direction. Henceforth, we focus on the SG force in this direction. Under the Frenkel model, according to Eq. (8), the spin-induced force in the y direction can be deduced as

$$F_{\text{SG-}y}^{\text{Frenkel}} = \frac{-Aes_z(B_0 + v_xE_0/c^2)(E_0 + v_xB_0)\cos(2\omega_Lt)}{m - As_z(B_0 + v_xE_0/c^2)\sin(\omega_Lt)} + \frac{eg_s\hbar[s_z\nabla_y(B_0 + v_xE_0/c^2)]/4}{m - As_z(B_0 + v_xE_0/c^2)\sin(\omega_Lt)}, \tag{14}$$

with the help of relations $dE_y/dt = \omega_LE_0\cos(\omega_Lt)$, $dB_z/dt = \omega_LB_0\cos(\omega_Lt)$, and $\gamma v_y = -e(E_0 + v_xB_0)\cos(\omega_Lt)/m\omega_L$, where $A = \gamma g_s\hbar e/4mc^2$ and where $\omega_L = -(1 + v_x/c)\omega_0$ can be understood as the frequency of the laser in electronic coordinates. It can be seen from Eq. (14) that when $a_0, \gamma \gg 1$, the first term is approximately proportional to $\gamma a_0^2s_z\hbar mc/2M\lambda^2$, which is significantly larger than the second term ($\sim a_0\hbar s_zmc/2M\lambda^2$) and shows asymmetric oscillations over time, where λ is the wavelength of the laser and $M = m - As_z(B_0 + v_xE_0/c^2)\sin(\omega_Lt)$ represents the spin-induced effective mass. Thus a net increment in the y component of the electron momentum will be obtained by integration over time. Consequently, the SG force in the Frenkel model will make electrons with opposite spins gradually acquire the opposite momentum in the y direction.

On the other hand, when the noncovariant DK model is adopted, similarly, after theoretical derivations in Sec. II C, from Eq. (12), we obtain the SG force in the y direction as

$$F_{\text{SG-}y}^{\text{DK}} = \frac{e\hbar s_z}{2m}\nabla_y\left[\left(a + \frac{1}{\gamma}\right)B_0 + \left(a + \frac{1}{\gamma+1}\right)\frac{v_xE_0}{c^2}\right]\times\sin(\omega_Lt) - \frac{e^2}{m^2}\frac{\hbar}{2}\frac{\gamma^2}{c^2}s_z\left[\frac{B_0}{\gamma^2} + \frac{v_xE_0}{(\gamma+1)^2c^2}\right] \times(E_0 + v_xB_0)\cos(2\omega_Lt) + \frac{e^4}{m^4}\frac{\hbar}{2}\frac{1}{c^6}\frac{v_xs_z}{2(1+\gamma)^3\omega_L^2}E_0^2(E_0 + v_xB_0)^2\sin^2(2\omega_Lt). \tag{15}$$

In Eq. (15), when $a_0, \gamma \gg 1$, the first and third terms are approximately proportional to $a_0s_z\hbar c/2\gamma\lambda^2$ and $a_0^4cs_z\hbar/2\lambda^2\gamma^3$, respectively, while the second term is approximately proportional to $a_0^2cs_z\hbar/2\lambda^2$, which is far larger than the other two terms, so its contribution is dominant. Hence we can see that the SG force caused by the noncovariant DK model is almost a simple harmonic oscillation $\sim\cos(2\omega_Lt)$. After integration over time, the SG force will not lead to any change in momentum in the y direction. It should be noted that the term related to the spin precession in the motion equation of the noncovariant DK model is neglected here. This is because the direction of electron spin is parallel or antiparallel to the z axis and $\boldsymbol{\Omega} \sim q\{(a + 1/\gamma)\mathbf{B} - [a + 1/(\gamma+1)]\boldsymbol{v}\times\mathbf{E}/c^2\}/m$ is also approximately along the z axis; hence the effects due to electron spin precession on its motion can be safely ignored according to Eq. (10).

According to Eqs. (14) and (15), with $\omega_L = -2\omega_0$, temporal evolutions of the SG forces on electrons with opposite spins for different energies γ and laser amplitudes a_0 are plotted in Figs. 2(a) and 2(b) for the Frenkel model and Figs. 2(e) and 2(f) for the noncovariant DK model. It is worth mentioning that terms related to the spatial gradient of fields in Eqs. (14) and (15) are ignored here, since it can be proved that they are much smaller than the other terms. Firstly, it can be seen that electrons with opposite spin states (red curves for spin up, black curves for spin down) are subjected to the opposite transverse SG force under both models. However, the SG force presents an asymmetric oscillation over time for the Frenkel model, while it shows a simple harmonic oscillation pattern for the noncovariant DK model. By comparing the cases of $\gamma = 800$ (solid curves) and $\gamma = 1000$ (dashed curves) in Fig. 2(a) for the Frenkel model, where $a_0 = 80$ is fixed, we can see that by increasing γ, a larger SG force is obtained. Correspondingly, when $\gamma = 800$ is fixed, the cases of $a_0 = 80$ (solid curves) and $a_0 = 100$ (dashed curves) shown in Fig. 2(b) reveal that the larger laser intensity also increases the SG force. These results are consistent with the analysis that the first term of Eq. (14) is approximately proportional to $\gamma a_0^2s_z\hbar mc/2M\lambda^2$. In contrast, for the noncovariant DK model, the oscillation term (the second term) in Eq. (15) is approximately proportional to a_0^2 and is significantly larger than the accumulation one (the third term), leading to the SG force being almost unaffected by γ while increasing with the growth of a_0, as shown in Figs. 2(e) and 2(f).

Furthermore, the momentum accumulated in the y direction derived by integrating the SG force from $t = 0$ to $t = T_0$ under various a_0 and γ for electrons with $s_z = \pm1$ is displayed

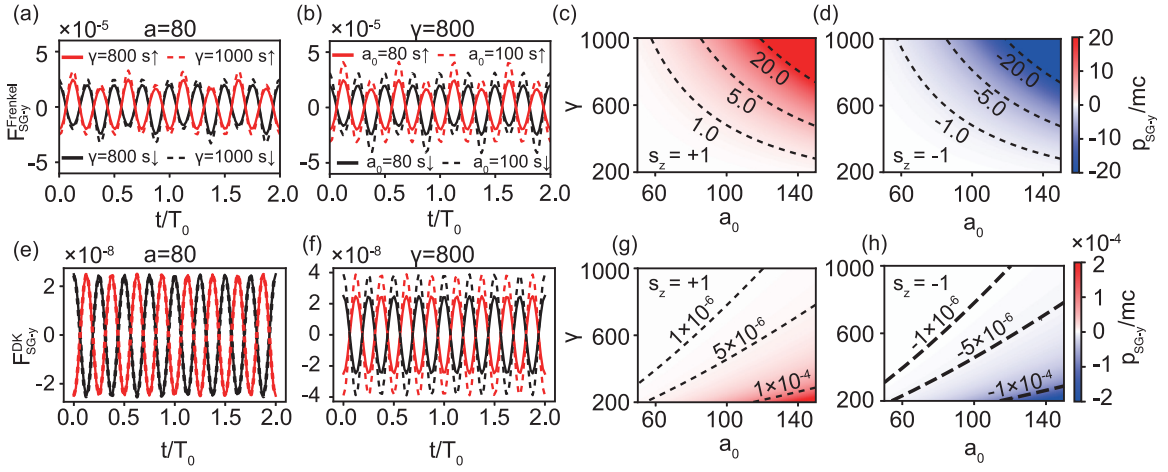

FIG. 2. (a) According to the first term of Eq. (14) in the Frenkel model, time evolution of the SG force in the y direction on electrons with opposite spin (red curves for $s_z = +1$ and black curves for $s_z = -1$) and different γ, where the laser amplitude is fixed as $a_0 = 80$. (b) The corresponding time evolutions for different a_0, where the Lorentz factor of the electron is fixed as $\gamma = 800$. (c) The momentum accumulated in the y direction derived by integrating Eq. (14) from $t = 0$ to $t = T_0$ under various laser intensities a_0 and various electron energies γ for an electron with spin $s_z = +1$. (d) The corresponding momenta for an electron with spin $s_z = -1$. (e)–(h) Same as (a)–(d), respectively, but according to the second and third terms of Eq. (15) in the noncovariant DK model [(e) and (f) have the same curve colors as in (a) and (b)].

in Figs. 2(c) and 2(d) for the Frenkel model and Figs. 2(g) and 2(h) for the noncovariant DK model, respectively. On the one hand, it shows that SG forces will cause electrons with opposite spin states to accumulate opposite momenta in both models; on the other hand, the magnitude of the accumulated momentum in the Frenkel model increases with increases in a_0 and γ and reaches up to the order of $10m_ec$; nevertheless, in the noncovariant DK model, the magnitude is five orders smaller than that in the Frenkel model and decreases with the growth of γ.

III. SIMULATION RESULTS

In order to confirm the theoretical analysis, simulations of the scheme shown in Fig. 1(a) were carried out using the 3D PIC code EPOCH [51] with the module for taking SG forces and the T-BMT equation into account. The accuracy of our spin-related module is confirmed by reproducing single-particle results of the Frenkel model (see Appendix B). The probe Gaussian laser with peak intensity $I_0 = 1.38\times10^{22}$ W/cm^2 ($a_0 = 80$), wavelength $\lambda = 0.8$ μm, $\sin^2$ temporal profile with duration $\tau = 30T_0$ ($T_0 = 2.67$ fs), and focal radius $r_0 = 2\lambda$ is incident from the left boundary into a $30\lambda\times24\lambda\times24\lambda$ simulation box, whose mesh size is $\lambda/20$. After a time delay of $15T_0$, an electron beam with density $n_e = 1.7\times10^{-19}$ cm^{-3}, length $l_e = 0.2\lambda$, diameter $d_e = 0.1\lambda$, and Gaussian energy distribution with a central Lorentz factor $\gamma_0 = 800$ and spread $\Delta\gamma = 50$ enters the simulation box and collides with the probe laser, which is modeled by 160 000 quasiparticles. The spin of the electrons is described by a vector $\mathbf{s} = (\sin\theta\cos\phi, \sin\theta\sin\phi, \cos\theta)$, and the beam is initially unpolarized, which means that spins of electrons are isotropically distributed on the "spin sphere," as shown in Fig. 1(d); it is natural to set $\theta = \arccos(2R_1 - 1)$ and $\phi = 2\pi R_2$, where $R_1, R_2 \in [0, 1]$ are random numbers.

The main results of the simulations are shown in Fig. 3. As mentioned earlier, we mainly focus on the SG force and

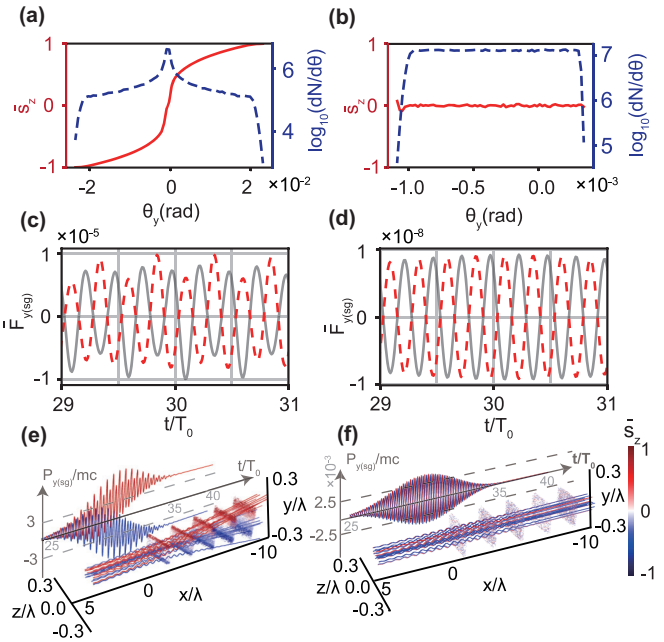

FIG. 3. Three-dimensional PIC simulation results: (a) The averaged spin $\bar{s}_z$ (red solid curve) and density (blue dashed curve) of electrons that distributed various intervals of θ_y under the Frenkel model, where $\theta_y = \arctan(p_y/p_x)$. (c) Time evolution of averaged SG force in the y direction for electrons with opposite spins dominated by the Frenkel model. (e) Forty typical electron trajectories in real space (x, y, z), where the colors of the trajectories denote the spin state of electrons, red for spin up ($s_z > 0$) and blue for spin down ($s_z < 0$); isosurface distributions for polarization of the electron beam at $t = 30, 32, 34, 36, 38T_0$, where the color bar displays the polarization of the isosurface distributions. The projection diagram shows the time evolution of the accumulated momentum in the y direction by the SG force for electrons with opposite spins dominated by the Frenkel model. (b), (d), and (f) Same as (a), (c), and (e), respectively, but for the noncovariant DK model.

momentum in the y direction, as well as the s_z, which marks the polarization states of electrons. When the initial unpolarized electron beam collides with the laser, electrons with opposite spins get opposite deflection angles in the y direction due to the effect of the SG force in the Frenkel model and then separate, as shown by the transverse angular distribution of polarization of the electron beam (red solid curve) in Fig. 3(a). If the noncovariant DK model is used, this phenomenon does not appear [see the red solid curve in Fig. 3(b)]. At this time, the motion of electrons in the polarization direction of the laser is mainly dominated by the ponderomotive force rather than the SG force, which induces an overall shift of the electron density distribution towards $\theta_y < 0$, as shown by the blue dashed curve in Fig. 3(b). For the Frenkel model, the effect of the ponderomotive force is overwhelmed, and the SG force broadens the density distribution with respect to θ_y; see the blue dashed curve in Fig. 3(a). (Detailed discussions of the influence of the ponderomotive force are given in Appendix C.)

To further understand the underlying physical causes of these phenomena, the time evolutions of the averaged SG forces in the y direction are traced in different cases, as shown in Figs. 3(c) and 3(d). It can be seen that both models predict that at any given time, electrons with opposite spins (red dashed curve for $s_z > 0$ and gray solid curve for $s_z < 0$) are subjected to SG forces in opposite directions. However, the magnitudes and time evolution patterns of SG forces predicted by different models vary greatly. When using the Frenkel model [see Fig. 3(c)], the asymmetric oscillation of the SG force with time causes the cumulative effect that electrons with different spins get opposite momenta in the y direction. This can be directly seen from the time evolution of the accumulated momentum by the SG force in the projection diagram in Fig. 3(e), which shows that, when the electrons move in the laser field for about $10T_0$, they can obtain momenta in the y direction with magnitude up to $\pm 4m_e c$. As a result, after interacting with the laser, there is significant spatial separation in the y direction for electrons with opposite spins, as shown by the trajectories of typical electrons in Fig. 3(e). In contrast, for the noncovariant DK model [see Fig. 3(d)], the approximately harmonic oscillation of the SG force makes the integral of the SG force in time be close to zero, leading to the disappearance of the phenomenon of separation [see Fig. 3(f)]. Meanwhile, Figs. 3(e) and 3(f) also display the isosurface distribution of the polarization of the electron beam at different times, which clearly shows the discrepancy between the Frenkel and noncovariant DK models. These results are in good agreement with the theoretical analysis in Sec. II D.

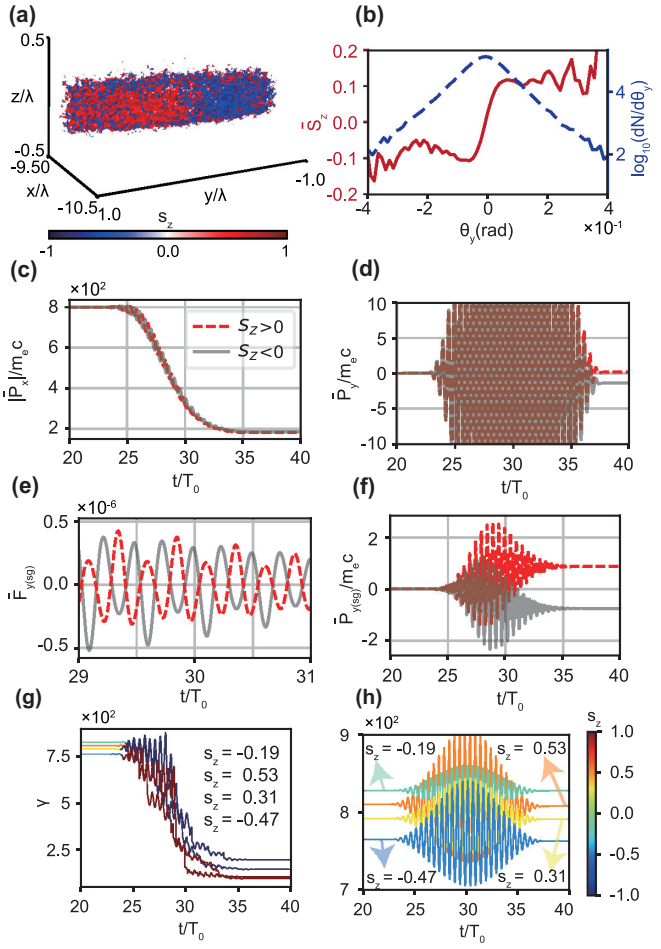

FIG. 4. Three-dimensional PIC simulation results with consideration of radiation under the Frenkel model: (a) Isosurface distribution for polarization s_z of the electron beam after interactions. (b) The averaged spin $\bar{s}_z$ (red solid curve) and density (blue dashed curve) of electrons that distributed various intervals of θ_y. (c) and (d) Time evolution of $|\bar{P}_x|/m_e/c$ and $\bar{P}_y/m_e/c$, respectively, for electrons with opposite spins. (e) and (f) Time evolution of the averaged SG force in the y direction and accumulated momentum by it, respectively, in the y direction for electrons with opposite spins. (g) Time evolution of γ of typical electrons, where the color of curves represents the evolutions of s_z of the electrons. (h) Same as (g), but for the case without taking radiation into account.

IV. IMPACT OF QUANTUM RADIATION EFFECTS

As we know, a relativistic electron emits photons randomly in the ultraintense laser, which inevitably affects its motion and spin. Only the Frenkel model is discussed here; we apply the quantum synchrotron radiation model [33,52], where the correction to the radiation probability induced by spin, the Sokolov-Ternov (ST) effect [53], and RR are taken into account in simulations. Figure 4(a) shows the isosurface distribution of polarization of scattered electrons. It can be seen that scattered electrons are still divided into two parts with opposite polarizations, although the degree of polarization has decreased compared with the case without consideration of the radiation effect, as shown by the red solid curve in Fig. 4(b). Such results are attributed to both RR and the ST effect.

We know that the RR force is much larger than the SG force [54], but for the parameters currently considered ($\gamma \gg a_0$), the former is basically longitudinal, as reflected by time evolutions of longitudinal and transverse momenta in Figs. 4(c) and 4(d). Thus the separation of polarized electrons caused by the SG force is not significantly changed by the RR force. Nevertheless, due to emissions of photons, electrons do lose energy gradually, resulting in reductions in the transverse SG force and the accumulated transverse momentum for the proportional relation between SG forces and γ of electrons, as shown by comparing Figs. 4(e) and 4(f) with Fig. 3(c)

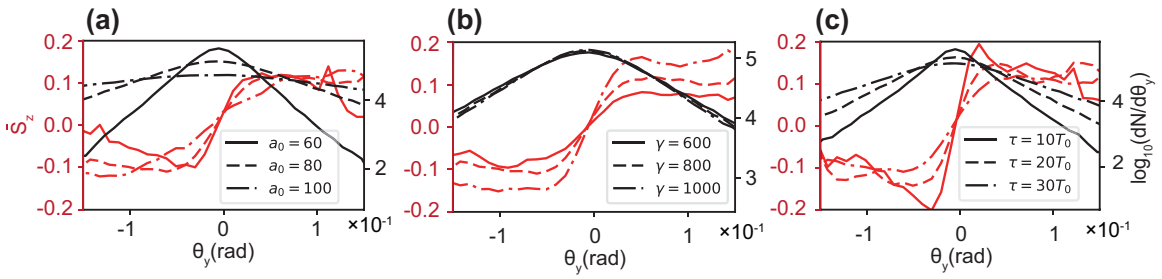

FIG. 5. Impacts of the (a) laser amplitude a_0, (b) initial energy of the electron beam γ, and (c) laser duration τ on the transverse angular distribution for density (black curves) and polarization (red curves) of the electron beam after interacting with the probe laser. In (a), the solid, dashed, and dash-dotted curves represent the cases $a_0 = 60$, $a_0 = 80$, and $a_0 = 100$, respectively. In (b), the solid, dashed, and dash-dotted curves represent the cases $\gamma = 600$, $\gamma = 800$, and $\gamma = 1000$, respectively. In (c), the solid, dashed, and dash-dotted curves represent the cases $\tau = 10T_0$, $\tau = 20T_0$, and $\tau = 30T_0$, respectively. Other parameters of the probe laser and electron beam are the same as those in Fig. 3.

and the projection diagram of Fig. 3(e). Figures 4(g) and 4(h) plot the evolution of the Lorentz factor γ and spin s_z of typical electrons with and without consideration of radiation effects, respectively. We see that the evolution of spin is dominated by the ST effect rather than the T-BMT equation in Fig. 4(g). According to the quantum radiation model applied here [33], once the electron emits a photon, its spin flips into the direction of $\boldsymbol{\beta}\times\hat{\boldsymbol{a}}$, where $\hat{\boldsymbol{a}}$ means the acceleration of the electron. In our scheme, this direction is almost kept in the z direction. Thus, after interacting with the laser, electrons with randomly distributed spin polarization direction collapse into states of $s_z = \pm 1$, which actually favors electrons to obtain greater transverse SG force compared with that for $|s_z| < 1$ [see Eq. (14)]. However, it is necessary to control the number of emitted photons $N_{ph} \sim a_0\alpha\tau/T_0$ [33,55], where α is the fine-structure constant, so as to ensure that the transverse momentum induced by the SG force is accumulated in the same direction during interactions.

V. IMPACT OF PARAMETERS OF THE LASER AND ELECTRON BEAM

It is also worth having a discussion about how parameters of the probe laser and the electron beam influence the final polarization and density distribution for the Frenkel model, where the radiation effect is taken into account. Here, we focus on laser amplitude a_0, initial energy γ of the electron beam, and laser duration τ.

Firstly, cases of different amplitudes a_0 are shown in Fig. 5(a). It can be seen that there is a larger angular dispersion for the density distribution of the electron beam by increasing a_0 [see black curves in Fig. 5(a)]. However, the maximum polarization is almost unchanged although the SG force becomes larger with the growth of a_0 according to the theoretical analysis [see Fig. 2(b)], which results from the fact that the transverse RR force comes significantly into play so that the influence of the SG force is submerged [see red curves in Fig. 5(a)]. In addition, the increase in a_0 leads to enhancement of the number of emitted photons ($N_{ph} \sim a_0\alpha\tau/T_0$), causing the spin state of the electrons to flip multiple times between $s_z = \pm 1$ and the polarization of the electron beam to decrease.

Figure 5(b) plots the results of cases in which the electron beam has various initial energies. It clearly shows that the maximum value of polarization becomes higher while the angular distribution of density is nearly unaffected when γ increases from 600 to 1000. This can be understood from the fact that the increased electron energy makes the ponderomotive force and the transverse RR force less important, while the influence of the SG force becomes prominent.

Finally, the influence of the laser duration is shown in Fig. 5(c). Apparently, the longer interaction time between the electron beam and the probe laser leads to greater transverse momentum accumulated by the electrons. Therefore the transverse angular distribution of density becomes wider with the growth of τ [see black curves in Fig. 5(c)]. On the other hand, when τ decreases, the electron beam can be divided into two parts with higher polarization [see red curves in Fig. 5(c)], because the number of photons radiated $N_{ph} \propto \tau$ is reduced and the ST effect is suppressed.

VI. CONCLUSION

In summary, the influence of spin-induced force on dynamics of relativistic electrons based on two different semiclassical models, the Frenkel model and the noncovariant DK model, has been studied. We found that the description of the influence of the spin-induced force on the trajectory of the electron is widely divergent under various models, which stem from different considerations or approximations applied in their establishment. Using 3D PIC simulations with a module for modeling the relativistic particle with spin motion, we have shown that it is possible to use ultraintense lasers to test currently existing theories on relativistic spin dynamics, so as to find the proper relativistic equations that describe both the evolution of spin and its influence on the motion of a particle with spin.

ACKNOWLEDGMENTS

This work is supported by Science Challenge Project, No. TZ2018005; National Natural Science Foundation of China, Grants No. 11825502, No. 11921006, and No. 12075014; the Strategic Priority Research Program of Chinese Academy of Sciences, Grant No. XDA25050900; and the National Key R&D Program of China, Grant No. 2016YFA0401100. B.Q. acknowledges support from National Natural Science Funds for Distinguished Young Scholars, Grant No. 11825502. The simulations were carried out on the Tianhe-2 supercomputer at the National Supercomputer Center in Guangzhou.

APPENDIX A: OTHER RELATIVISTIC SPIN MODELS BASED ON RELATIVISTIC GENERALIZATION OF THE NONRELATIVISTIC SPIN MODEL

In general, there are two avenues for establishing a relativistic semiclassical model that describes the evolution of spin and its influence on the motion of a particle. On the one hand, some semiclassical models can be derived based on relativistic generalization of the nonrelativistic semiclassical spin model that stems from the classical correspondence of QM [16–18]. On the other hand, one can proceed from the relativistic QM and obtain the equation of momentum or spin by employing the semiclassical approximation and correspondence principle to the Heisenberg equations [30,32].

Nevertheless, there is no universally accepted spin operator in the relativistic regime, resulting in obscureness of those spin-related theories starting from relativistic QM. Therefore we prefer to pay more attention to more intuitive semiclassical models derived from relativistic generalizations of the nonrelativistic semiclassical spin model, because the problem of the nonunique relativistic spin operator is circumvented. Furthermore, since there are explicit connections between the classical spin vector in the rest frame and its relativistic generalizations (four-vector S^{μ} and four-tensor $S^{\mu\nu}$), it is more convenient for these models to be further implemented into many-particle simulations, e.g., PIC code, so that we can demonstrate realistically the potential experimental scheme while considering the collective effect of charged particles, quantum RR, the ST effect, and so on. In fact, there are lots of semiclassical models that give different forms of relativistic equations describing the effect of spin on the motion of particles, and these differences actually result from different considerations when these models are established. Of necessity, they can be consistent with each other when the same considerations are applied. Here, several commonly used models are recalled, and their differences and relations to the Frenkel model and noncovariant DK model are illustrated.

1. Covariant Derbenev-Kondratenko model stemming from changing the notion of the particle coordinate

Just as in the noncovariant DK model in Sec. II C, $H_{\rm int}^{\rm eff}$ in Eq. (11) is considered as the Hamiltonian of the interaction between spin and the EM fields in the relativistic regime. If it is assumed that the relativistic spin-induced force is only related to the gradient of the EM fields, as in the nonrelativistic case, the equation of motion is given by the Lagrangian equation as [45]

$$m_0\frac{d(\gamma \boldsymbol{v})}{dt} = q(\mathbf{E}+\boldsymbol{v}\times\mathbf{B}) + \nabla(\mathbf{s}\cdot\boldsymbol{\Omega}). \tag{A1}$$

By changing the notion of the coordinate of the particle $r \to r + \frac{1}{m_0}\frac{\gamma}{\gamma+1}(\mathbf{s}\times\mathbf{v})$, one has proved that the above equation can be represented as a covariant form [45]:

$$\begin{aligned} m_0\dot{U}_\alpha = {} & qF_{\alpha\beta}U^\beta + \frac{qg_s}{4m_0}S^{\gamma\beta}\left(\partial_\alpha - \frac{1}{c^2}U_\alpha U^\sigma\partial_\sigma\right)F_{\gamma\beta} \\ & - \frac{g_s q}{4m_0c^2}S^{\sigma\gamma}F_{\sigma\gamma}F_{\alpha\beta}U^\beta - \frac{q^2(g_s-2)^2}{4m_0^2c^2}S_{\alpha\omega}F^{\omega}_{\beta}F^{\beta\alpha}U_\alpha \\ & + \frac{q(g_s-2)}{2m_0c^2}S^{\lambda}_{\alpha}(U_\sigma\partial^\sigma)F_{\lambda\alpha}U^\alpha \\ & + \frac{q^2g_s(g_s-2)}{4m_0^2c^2}F_{\alpha\omega}S^{\omega}_{\beta}F^{\beta\lambda}U_\lambda, \end{aligned} \tag{A2}$$

where the condition $U_\alpha\dot{U}^\alpha = 0$ is satisfied, according to $S_{\alpha\beta}U^\alpha = 0$, $U_\alpha U^\alpha = c^2$, and $U^\gamma F_{\gamma\alpha}S^{\alpha\beta}F_{\beta\sigma}U^\sigma = 0$ [22].

Apparently, compared with the covariant equation of motion [Eq. (5)] in the Frenkel model in Sec. II B, the covariant DK model contains only the effect of the first order of spin. When applying the same approximation, it can be proved that Eq. (5) of the Frenkel model is identical to Eq. (A2) of the covariant DK model, i.e., substituting $\dot{U}_\gamma = \frac{q}{m_0}F_{\gamma\alpha}U^\alpha$ into a_γ and the term related to spin-induced effective mass in Eq. (5):

$$a_\gamma = -\frac{g_s-2}{2c^2}F_{\gamma\alpha}U^\alpha, \tag{A3}$$

$$\dot{a}_\gamma = -\frac{g_s-2}{2c^2}\left[(U_\lambda\partial^\lambda)F_{\gamma\alpha}U^\alpha + \frac{q}{m_0}F_{\gamma\alpha}F^{\alpha\beta}U_\beta\right], \tag{A4}$$

$$M\dot{U}_\alpha = m_0\dot{U}_\alpha + \frac{\chi q}{2c^2m_0}S^{\beta\gamma}F_{\beta\gamma}F_{\alpha\lambda}U^\lambda. \tag{A5}$$

Meanwhile, $-\chi U_\alpha\dot{S}^{\beta\gamma}F_{\beta\gamma}/2c^2$ in R_α is neglected in order to satisfy the condition $U_\alpha\dot{U}^\alpha = 0$.

2. The covariant generalization of the equation of motion of a particle with spin in the rest frame

In the rest frame, the equation of motion of a particle with spin is determined by the well-known expression $m_0\frac{d\mathbf{v}}{dt} = q\mathbf{E} + \chi\nabla\mathbf{s}\cdot\mathbf{B}$. By taking the covariant generalization, another relativistic equation of motion of a particle with spin can be obtained as [22]

$$m_0\dot{U}_\alpha = qF_{\alpha\beta}U^\beta + \frac{\chi}{2}S^{\gamma\beta}\left(\frac{\partial}{\partial x^\alpha} - \frac{1}{c^2}U_\alpha U^\beta\frac{\partial}{\partial x^\beta}\right)F_{\gamma\beta}, \tag{A6}$$

where the introduction of $\frac{\partial}{\partial x^\alpha} - \frac{1}{c^2}U_\alpha U^\beta\frac{\partial}{\partial x^\beta}$ is to satisfy $U^\alpha\dot{U}_\alpha = 0$. Such an equation is commonly used in the derivation of the equation describing the evolution of spin [18–21]. It can be clearly seen that, in contrast with Eq. (7) of the Frenkel model, the influence of the effective mass is not taken into account in the above equation, i.e., $M = m_0$.

APPENDIX B: SIMULATIONS OF MOTION OF ELECTRONS WITH SPIN IN AN ULTRAINTENSE LASER AND HOMOGENEOUS MAGNETIC FIELD BASED ON THE FRENKEL MODEL

To confirm the accuracy of our PIC module for modeling the motion of relativistic particles with spin, by considering the Frenkel model, we reproduce the motion of electrons with spin in an ultraintense laser or homogeneous magnetic field, which was achieved by single-particle simulations in previous literature [46,56].

Firstly, simulations of the collision between a LP laser with amplitude $E_y = 2.57\times10^{15}$ V/m, wavelength $\lambda = 1.06$ nm, and $\sin^2$ temporal profile with $\tau = 6T_0$ and electrons with opposite spins and different initial momenta are carried out, where the parameters of the electrons and laser are the same

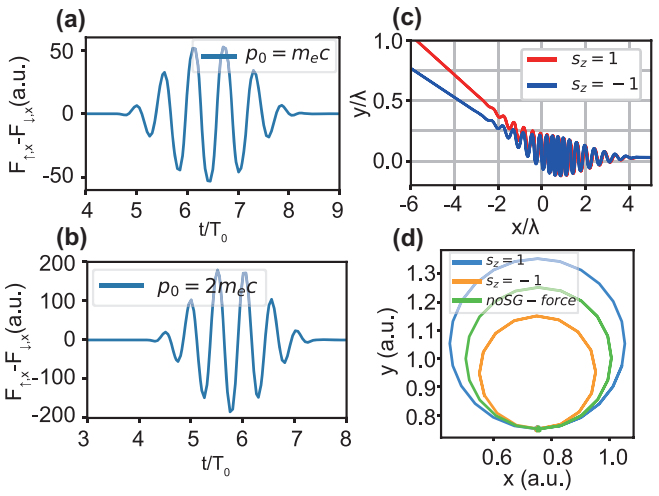

FIG. 6. Three-dimensional simulation results as a benchmark against which the results of previous publications (Refs. [46,56]) can be compared. (a) and (b) Difference of the SG force components in the direction of laser propagation (x) subjected by two electrons with opposite spin ($s_z = \pm 1$) and initial momentum of (a) $p_0 = (-m_e c, 0, 0)$ and (b) $p_0 = (-2m_e c, 0, 0)$ during the interaction with a LP laser pulse. (c) Trajectories of electrons with opposite spins in a LP focused laser. (d) Trajectories of electrons with initial momentum of $3.56 m_e c$ in a homogeneous magnetic field with strength of 4.7×10^8 T, with (blue curve for a spin-up electron and orange curve for a spin-down electron) and without (green curve) consideration of the SG force.

as those in Ref. [46]. Figures 6(a) and 6(b) show the difference of the SG force components in the direction of laser propagation (x) for two electrons with opposite spin ($s_z = \pm 1$) when their initial momenta are $p_0 = (-m_e c, 0, 0)$ and $p_0 = (-2m_e c, 0, 0)$, respectively. It can be seen that electrons with opposite spins are subjected to opposite SG forces and the difference becomes larger with the increase in the initial momentum of the electron. These results match the results in Figs. 1(c) and 1(d) in Ref. [46].

Secondly, two electrons with opposite spins are used to collide with a focused LP laser, where the Lorentz factor of the electrons is $\gamma = 100$ and the amplitude, wavelength, duration, and focus radius are $E_y = 8.03\times10^{14}$ V/m, $\lambda = 0.8\ \mu$m, $\tau = 20T_0$, and $w_0 = 2\lambda$, respectively. The trajectories of these two electrons are plotted in Fig. 6(c), which clearly shows that there is a divergence angle (aberration angle) between electrons with opposite spins after interacting with the focused laser. This is consistent with Fig. 3 in Ref. [46].

Finally, we also consider the motion of electrons in a homogeneous magnetic field, where the gradient force of the Frenkel model vanishes and only the effect of spin-induced effective mass is retained. The momentum of the electrons and the strength of the homogeneous magnetic field are chosen as $p_x = 3.56 m_e c$ and $B_z = 4.7\times10^8$ T, respectively, which are the same values as those in Ref. [56]. When the SG force is not taken into account, the electrons have cyclotron motion, as shown by the green curve in Fig. 6(d). Meanwhile, the trajectories of electrons with $s_z = 1$ and $s_z = -1$ are plotted by a blue curve and an orange curve in Fig. 6(d), respectively, where changes in the radius of the trajectories associated with SG forces are identical to those shown in Fig. 1 in Ref. [56].

APPENDIX C: INFLUENCE OF PONDEROMOTIVE FORCE

Due to the utilization of a focused probe laser in our scheme, it is necessary to discuss the influence of transverse ponderomotive force in different models. At first, as we know, the ponderomotive force in the noncovariant DK model can be expressed as $F_p \sim a_0^2 mc^2/\lambda\gamma$, which is much larger than the accumulation term ($\sim a_0^4 \hbar s_z c/2\gamma^3\lambda^2$) of Eq. (15) when $a_0^2/\gamma^2 \ll 10^5$, where $\lambda \sim 10^{-6}$ m. Such a condition is always satisfied in our scheme because $a_0 \ll \gamma$; this limit ensures that electrons cannot be accelerated backward by the ultraintense laser and makes the radiation reaction force be mainly in the longitudinal direction. Thus it is inevitable that the influence of the SG force on the trajectories of the electrons is overridden by that of the ponderomotive force in the noncovariant DK model. However, under the Frenkel model, the ponderomotive force is corrected by the spin-related effective mass as $F_p \sim a_0^2 m^2 c^2/M\lambda\gamma$, which is comparable to the SG force when $\gamma^2 \sim 10^5$. Consequently, combined with the theoretical analysis in Sec. II, the SG force under the Frenkel model can force electrons with opposite spins to gradually acquire opposite transverse momentum and, in addition, is large enough to realize spatial separation of electrons with opposite polarization.

[1] D. Strickland and G. Mourou, Opt. Commun. **55**, 447 (1985).
[2] ELI Delivery Consortium, https://eli-laser.eu/.
[3] C. Hernandez-Gomez, S. P. Blake, O. Chekhlov, R. J. Clarke, A. M. Dunne, M. Galimberti, S. Hancock, R. Heathcote, P. Holligan, A. Lyachev, P. Matousek, I. O. Musgrave, D. Neely, P. A. Norreys, I. Ross, Y. Tang, T. B. Winstone, B. E. Wyborn, and J. Collier, J. Phys.: Conf. Ser. **244**, 032006 (2010).
[4] www.xcels.iapras.ru
[5] W. Li, Z. Gan, L. Yu, C. Wang, Y. Liu, Z. Guo, L. Xu, M. Xu, Y. Hang, Y. Xu, J. Wang, P. Huang, H. Cao, B. Yao, X. Zhang, L. Chen, Y. Tang, S. Li, X. Liu, S. Li *et al.*, Opt. Lett. **43**, 5681 (2018).
[6] L. H. Thomas, Nature (London) **117**, 514 (1926).
[7] J. D. Jackson, Rev. Mod. Phys. **48**, 417 (1976).
[8] I. M. Ternov, V. G. Bagrov, and A. M. Khapaev, Ann. Phys. (Berlin) **477**, 25 (1968).
[9] V. B. Berestetskii, L. D. Landau, E. M. Lifshitz, and L. Pitaevskii, *Quantum Electrodynamics*, Course of Theoretical Physics Vol. 4 (Butterworth-Heinemann, Oxford, 1982).
[10] L. D. Landau and E. M. Lifshitz, *Quantum Mechanics: Non-relativistic Theory*, Course of Theoretical Physics Vol. 3 (Elsevier, Oxford, 2013).
[11] R. Ekman, F. A. Asenjo, and J. Zamanian, Phys. Rev. E **96**, 023207 (2017).
[12] A. A. Deriglazov and W. G. Ramírez, Adv. Math. Phys. **2017**, 7397159 (2017).

[13] B. Średniawa, in *Cosmology and Gravitation: Spin, Torsion, Rotation, and Supergravity*, edited by P. G. Bergmann and V. De Sabbata (Springer, Boston, 1980), pp. 423–434.

[14] R. Mondal and P. M. Oppeneer, J. Phys.: Condens. Matter **32**, 455802 (2020).

[15] A. A. Pomeranskii and I. B. Khriplovich, J. Exp. Theor. Phys. **86**, 839 (1998).

[16] J. Frenkel, Z. Phys. **37**, 243 (1926).

[17] V. S. Derbenev and A. M. Kondratenko, Sov. Phys. JETP **37**, 6 (1973).

[18] R. H. Good, Phys. Rev. **125**, 2112 (1962).

[19] K. Rafanelli, Nuovo Cimento A **67**, 48 (1970).

[20] A. I. Solomon, Nuovo Cimento **26**, 1320 (1962).

[21] P. Nyborg, Nuovo Cimento **31**, 1209 (1964).

[22] I. M. Ternov and V. A. Bordovitsyn, Sov. Phys.-Usp. **23**, 679 (1980).

[23] H. Bauke, S. Ahrens, C. H Keitel, and R. Grobe, New J. Phys. **16**, 043012 (2014).

[24] H. Bauke, S. Ahrens, C. H. Keitel, and R. Grobe, Phys. Rev. A **89**, 052101 (2014).

[25] K. Y. Bliokh, M. R. Dennis, and F. Nori, Phys. Rev. A **96**, 023622 (2017).

[26] L. Zou, P. Zhang, and A. J. Silenko, Phys. Rev. A **101**, 032117 (2020).

[27] S. M. Barnett, Phys. Rev. Lett. **118**, 114802 (2017).

[28] I. A. Aleksandrov, D. A. Tumakov, A. Kudlis, V. M. Shabaev, and N. N. Rosanov, Phys. Rev. A **102**, 023102 (2020).

[29] Y. Fu, Y. Liu, C. Wang, J. Zeng, and J. Yuan, Phys. Rev. A **100**, 013405 (2019).

[30] A. J. Silenko, Phys. Rev. A **77**, 012116 (2008).

[31] F. Fillion-Gourdeau, E. Lorin, and A. D. Bandrauk, Comput. Phys. Commun. **183**, 1403 (2012).

[32] T.-W. Chen and D.-W. Chiou, Phys. Rev. A **90**, 012112 (2014).

[33] Y.-F. Li, R. Shaisultanov, K. Z. Hatsagortsyan, F. Wan, C. H. Keitel, and J.-X. Li, Phys. Rev. Lett. **122**, 154801 (2019).

[34] D. Del Sorbo, D. Seipt, T. G. Blackburn, A. G. R. Thomas, C. D. Murphy, J. G. Kirk, and C. P. Ridgers, Phys. Rev. A **96**, 043407 (2017).

[35] C. Bœhm, C. Degrande, O. Mattelaer, and A. C. Vincent, J. Cosmol. Astropart. Phys. **2017**, 043 (2017).

[36] R. Erhard and H. Bauke, Phys. Rev. A **92**, 042123 (2015).

[37] F. Wan, R. Shaisultanov, Y.-F. Li, K. Z. Hatsagortsyan, C. H. Keitel, and J.-X. Li, Phys. Lett. B **800**, 135120 (2020).

[38] Y. Wu, L. Ji, X. Geng, Q. Yu, N. Wang, B. Feng, Z. Guo, W. Wang, C. Qin, X. Yan, L. Zhang, J. Thomas, A. Hützen, A. Pukhov, M. Büscher, B. Shen, and R. Li, Phys. Rev. E **100**, 043202 (2019).

[39] Y.-Y. Chen, P.-L. He, R. Shaisultanov, K. Z. Hatsagortsyan, and C. H. Keitel, Phys. Rev. Lett. **123**, 174801 (2019).

[40] Y.-F. Li, R.-T. Guo, R. Shaisultanov, K. Z. Hatsagortsyan, and J.-X. Li, Phys. Rev. Appl. **12**, 014047 (2019).

[41] M. Büscher, A. Hützen, L. Ji, and A. Lehrach, High Power Laser Sci. Eng. **8**, e36 (2020).

[42] W. Gerlach and O. Stern, Z. Phys. **8**, 110 (1922).

[43] J. Thomas, A. Hützen, A. Lehrach, A. Pukhov, L. Ji, Y. Wu, X. Geng, and M. Büscher, Phys. Rev. Accel. Beams **23**, 064401 (2020).

[44] H. Van Dam and T. Ruijgrok, Phys. A (Amsterdam) **104**, 281 (1980).

[45] K. Heinemann, arXiv:physics/9611001.

[46] M. Wen, H. Bauke, and C. H. Keitel, Sci. Rep. **6**, 31624 (2016).

[47] D. Tskhakaya, K. Matyash, R. Schneider, and F. Taccogna, Contrib. Plasma Phys. **47**, 563 (2007).

[48] A. Arda and R. Sever, Few-Body Syst. **58**, 7 (2017).

[49] W. Pauli, Rev. Mod. Phys. **13**, 203 (1941).

[50] J. D. Jackson, *Classical Electrodynamics*, 2nd ed. (Wiley, New York, 1975).

[51] T. D. Arber, K. Bennett, C. S. Brady, A. Lawrence-Douglas, M. G. Ramsay, N. J. Sircombe, P. Gillies, R. G. Evans, H. Schmitz, A. R. Bell, and C. P. Ridgers, Plasma Phys. Controlled Fusion **57**, 113001 (2015).

[52] D. Seipt, D. Del Sorbo, C. P. Ridgers, and A. G. R. Thomas, Phys. Rev. A **100**, 061402(R) (2019).

[53] A. A. Sokolov and I. Ternov, in *Doklady Akademii Nauk* (Russian Academy of Sciences, 1963), Vol. 153, pp. 1052–1054.

[54] D. Del Sorbo, D. Seipt, A. G. R. Thomas, and C. P. Ridgers, Plasma Phys. Controlled Fusion **60**, 064003 (2018).

[55] A. Di Piazza, C. Müller, K. Z. Hatsagortsyan, and C. H. Keitel, Rev. Mod. Phys. **84**, 1177 (2012).

[56] M. Wen, C. H. Keitel, and H. Bauke, Phys. Rev. A **95**, 042102 (2017).